J Mater Sci (2008) 43:1696–1700
DOI 10.1007/s10853-007-2376-1

Polymer–ITO nanocomposite template for the optoelectronic application

Sukti Chatterjee

Received: 17 September 2007 / Accepted: 3 December 2007 / Published online: 11 January 2008

Abstract Polymer–ITO (PI) nanocomposite templates with various ITO concentrations have been fabricated by electrospinning. These templates look like a mat with tangled nanofibers, and are optically transparent (85–90%) in the visible region of the solar spectrum (400–700 nm). The electronic properties of those transparent films were studied. The highest conductivity achieved is 1.04×10^3 S cm^{-1}. The promising optoelectronic properties present the great promise of PI nanocomposites to be the top layer of the next generation flexible photo devices, like solar cells and light emitting diodes (LED).

Introduction

Transparent conductive oxides (TCO) are widely used transparent conducting coating for optoelectronic devices such as flat panel displays, solar cells, and touch screens [1, 2]. Also, it is an essential material for the automotive, train, and aircraft industries. Therefore, the numerous research programs [3–7] are going on to develop TCO. Over the years of research, among the different TCO materials, viz. aluminum-doped zinc oxide (AZO, ZnO:Al), fluorine-doped tin oxide (FTO, SnO_2:F), antimony-doped tin oxide (ATO), and indium tin oxide (ITO), ITO with In:Sn = 9:1 (at.%) seem to be the most favorable due to their remarkable combination of high transparency in the visible region, high infrared reflectivity, and high conductivity. However, those ceramic TCO films are brittle, which is a mechanical limitation for their use in the flexible optoelectronic devices. Again, we could find the demanding use of plastic optoelectronic devices because of their ease of processing, mechanical flexibility, and promise for low-cost fabrication of large areas [1, 2]. Therefore, we need to take the challenge for finding out the substitute of commonly used TCO films.

For that particular task, a new class of nanostructured materials, e.g., polymer–carbon nanotubes (CNT), nanocomposite (NC), polymer–TCO nanocomposite, etc. were invented and studied by the different research groups [8–14]. These nanocomposites are composed of a continuous transparent polymer matrix homogeneously dispersed with nano-sized semiconductor particles. In fact, polymer matrix acts as a binder of the nanoparticles. The degree of uniform dispersion as well as the volume fraction of semiconductor nanoparticles control the optoelectronic properties of the nanocomposites. Clayton et al. [9] studied the optical transparency of poly(methyl methacrylate)/single-walled carbon nanotube (PMMA/SWNT) composite. Glatkowski and his research group [10] presented SWNT composite coating with optical transparency of 90% and electrical resistivity of 200 Ω/□ synthesized by simple wet coating processes. Like polymer–CNT nanocomposite, polymer–ITO nanocomposite is a promising alternate choice of TCO, too. Puetz et al. [13] investigated 3-methacryloxy propyltrimethoxysilane (MPTS)–ITO nanocomposites. The sheath resistances of UV-cured transparent MPTS-ITO NCs are in the range of 1–2 kΩ that makes an interest to apply the nanocomposites in the optoelectronic devices. The electrical and mechanical properties of transparent polyvinylpyrrolidone (PVP)–ITO nanocomposites

S. Chatterjee
Centre for Composite Materials, University of Delaware, Newark, DE 19716, USA

S. Chatterjee (✉)
Naval Materials Research Laboratory, Defense Research and Development Organization, Ambernath 421 506, India
e-mail: Sukti@yahoo.com

studied by Carotenuto et al. [14] are also encouraging for the technological applications.

In the present work, the customization of the properties of polymer–ITO nanocomposite has been studied. To serve the purpose, polyethylene oxide (PEO)–ITO nanocomposite templates were fabricated by electrospinning. The morphologies of PEO–ITO NCs were manipulated in a wide range. The morphological transformation has an effect on the optoelectronic properties of the templates. As a result, we obtained PI nanocomposite films with the extensive varieties of optoelectronic properties.

Experiments

Preparation of PI nanocomposite templates

Polymer–ITO nanocomposite templates were synthesized by electrospinning. The solutions used in the electrospinning experiments were prepared by using 400,000 molecular weight PEO (M_w: 400,000, Scientific Polymer Products) and ITO nanopowder (~40 nm) (Inframat® Advanced Materials™). Actually, ITO nanopowder (~40 nm) is a combination of In_2O_3 and SnO_2 in a ratio of 90:10. PEO was dissolved in the stable suspension of ITO in HPLC grade water. PEO concentration was always 8 wt% in water. ITO concentration was varied. Suspensions were prepared with ITO concentrations of 10, 20, 30, and 40% of the mass of dissolved PEO. After magnetic stirring for 6 h, the PEO–ITO solutions were loaded into a 50 ml plastic syringe equipped with an 18-gauge stainless steel needle (Popper & Sons, Inc.). A voltage of 9 kV was applied to the needle by a power supply (ES30P-5W, Gamma High Voltage Research, Ormond Beach, FL), while a syringe pump (KDS-200, Stoelting, Wood Dale, IL) fed the PEO–ITO solution at a constant rate of 0.3 mL/h. The PEO–ITO nanocomposite templates of different thicknesses were collected on various substrates, including aluminum foils, silicon wafers, glass slides, and lacy carbon-coated copper grids for different sorts of characterizations at a distance of 5 in. from the tip of the needle.

Characterizations

Transmission electron microscopy (TEM, JEM 2010F) was used to study the architectures of PI nanocomposite templates. The compositions and microstructures of templates were analyzed by different techniques: bright field (BF), high-angle annular dark field (HAADF), and energy dispersive X-ray spectroscopy (EDXS) of TEM. The morphologies of nanocomposite templates were determined by X-ray diffraction (XRD) measurements. XRD patterns were recorded on a Rigaku D-Max B horizontal diffractometer (Cu Kα radiation), and analyzed by JADE software [15]. To study the optical characteristics of PI template films, the coated glass substrates were subjected to the optical transmittance and reflectance measurements in the wavelength range of 200–1,000 nm by using UV–Vis–NIR Perkin Elmer spectrophotometer. A bare glass substrate was used as the optical reference. The conductivities of PI template thin films were measured using a four-point probe in an environmental test chamber.

Results and discussion

Structural studies

Figure 1 shows a typical TEM image of the PEO–ITO nanocomposite template. It is Z-contrast imaging [16], generated by HAADF scanning transmission electron microscopy (STEM). The PEO–PI nanocomposite template looks like a mat with tangled nanofibers. The average diameter of nanofibers is ~40 nm. The high-resolution HAADF images could help to distinguish the PEO–PI templates having different ITO concentrations due to their Z-contrast imaging capability. As for evidence, two high-resolution HAADF images of PEO–ITO templates having ITO concentrations of (a) 10% and (b) 40% have been displayed in Fig. 2. In Fig. 2b, the template looks like ITO

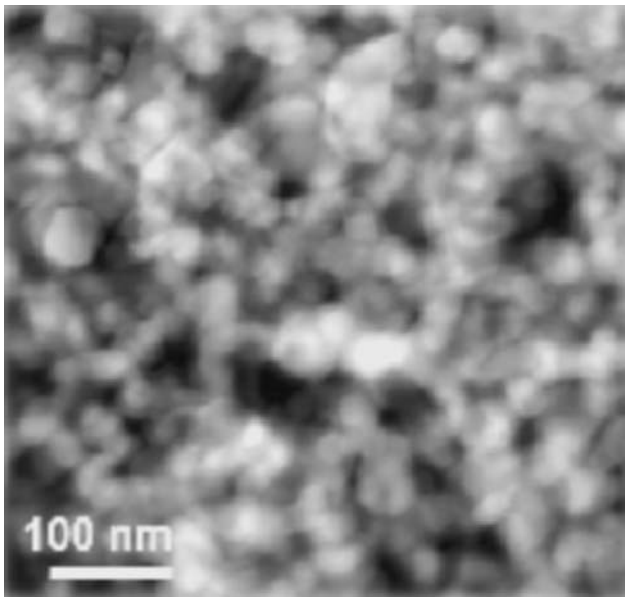

Fig. 1 Z-contrast imaging, generated by high-angle annular dark field (HAADF) scanning transmission electron microscopy (STEM) of PEO–PI nanocomposite template with ITO concentration of 30%

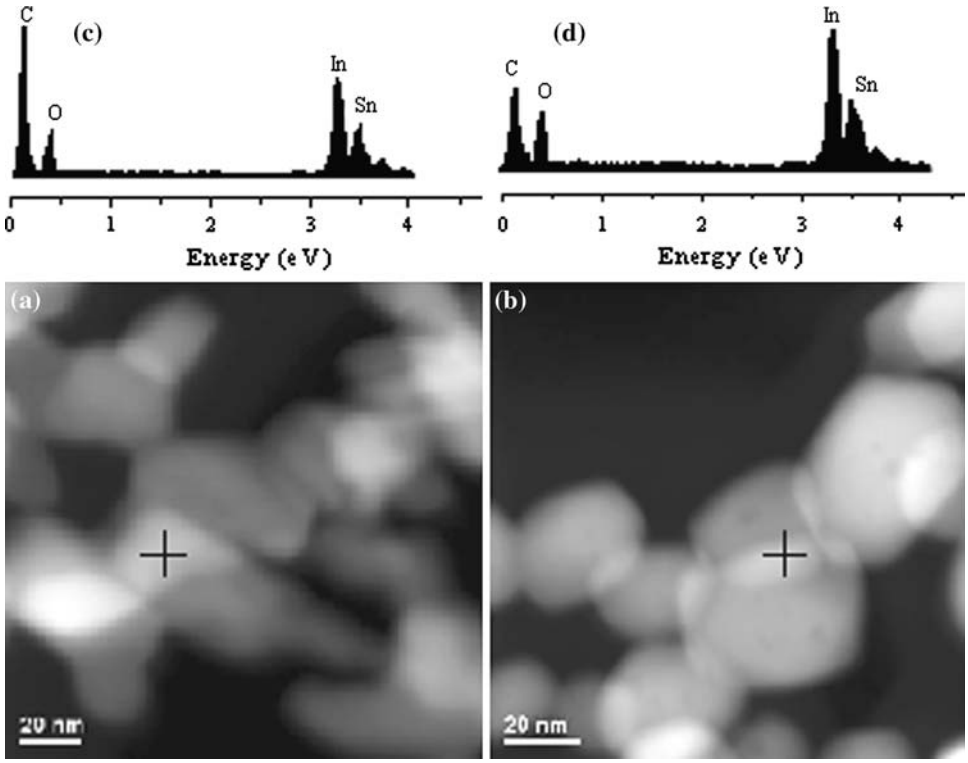

Fig. 2 High-resolution HAADF images of PEO–PI nanocomposite templates with ITO concentrations of (**a**) 10% and (**b**) 40%. (**c**) and (**d**) include EDXS spectra of corresponding nanocomposite templates

dominating, and ITO nanoparticles are seemed to be sorted in a network. On the other hand, blurry template in Fig. 2a indicates the predominating presence of polymer rather than inorganic nanoparticles. To support the fact, the compositions of two nanocomposite templates have been analyzed by EDXS. Fig. 2c, d display the energy dispersive X-ray spectra of PEO–PI templates with 10 and 40% ITO, respectively. The relative concentration of carbon is higher in the PEO–PI template with 10% ITO than that in the other template. It confirms the dominating presence of PEO over ITO nanoparticles in the PEO–PI template with 10% ITO.

Like the TEM study, the XRD patterns as well provide us with the morphological information of different PEO–PI templates. In Fig. 3, the XRD patterns of four PEO–PI templates with 10, 20, 30, and 40% ITO have been displayed. Figure 3 also includes the standard XRD peak positions of PEO, In_2O_3, and SnO_2. Curve 1, which corresponds to PEO–PI template with 10% ITO, shows crystalline peaks of PEO as well as In_2O_3. Here it should be mentioned that there is no evidence of the SnO_2 peaks in any of the curves. This could be caused by the small amount of SnO_2 in the ITO film. Presence of SnO_2 can be confirmed to study the Energy Dispersive X-ray spectra of PEO–PI templates (Fig. 2). With the increase in ITO concentration, diffraction peaks of PEO gradually disappear. These are barely present in the XRD pattern of PEO–PI template with 40% ITO (curve 4).

Optoelectronic properties

So far, the morphological studies show that we can easily tailor the concentration of ITO nanoparticles in the PEO–ITO templates. It is expected that the PI nanocomposites with different concentrations of ITO would have different optical and electrical properties. Figure 4 demonstrates the optical properties of the PEO–PI template films having the

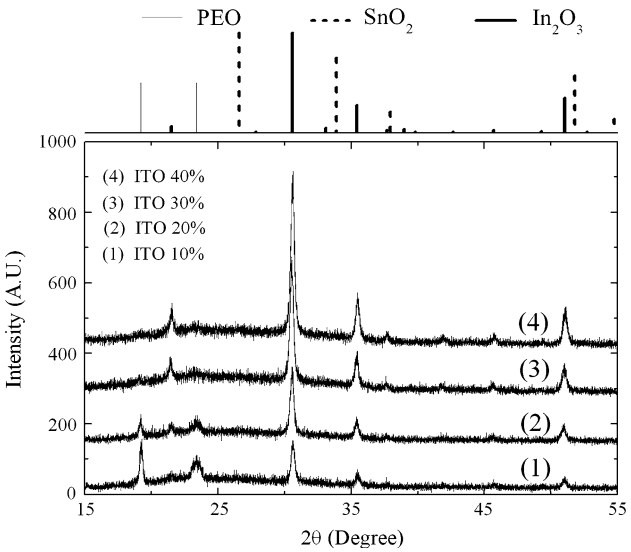

Fig. 3 XRD patterns of PEO–PI nanocomposite films with ITO concentrations of 10, 20, 30, and 40%

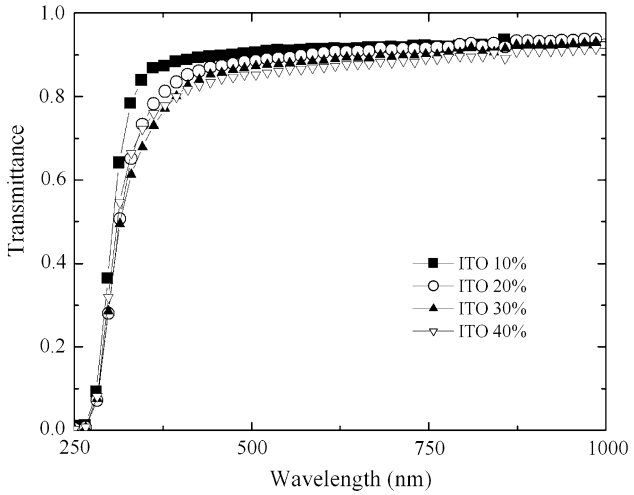

Fig. 4 Transmission spectra of PEO–PI nanocomposite films with ITO concentrations of 10, 20, 30, and 40%

same thickness of 150 nm. It is observed in the figure that the average transmission of PEO–PI template films in the visible region (400–700 nm) of solar spectrum is about 85–90%. The optical transmission above 550 nm hardly changes with the ITO concentration. The drop of optical transmission with the ITO concentration is relatively higher in the wavelength range of 250–500 nm. It varies from 5 to 10% at different wavelengths. This particular fall of optical transmission can be explained easily. The optical absorption edge of PEO is at ~260 nm [17, 18], and PEO is ~90% transparent in the UV–Vis–NIR region. On the other hand, ITO has the optical band edge at ~340 nm [18–21], and obviously its optical transmission starts to drop at ~400 nm, though its optical transparency in the visible region is like PEO. Consequently, the optical transmittance of the PEO–PI nanocomposite in the wavelength range of 250–500 nm lessens depending on the concentration of ITO. However, it is fascinating to mention that whatever the ITO concentration is, PEO–PI nanocomposites are transparent in the visible region, and that is crucial for its application in the optoelectronic devices.

The promising optical properties have encouraged for examining the electronic transport properties of PEO–PI nanocomposite templates. Conductivity (σ) is plotted against the ITO concentration in Fig. 5. It is exponentially increased with ITO concentration. At the ITO concentration of 40% conductivity of the PEO–PI nanocomposite is 1.04×10^3 S cm^{-1} while the reported conductivities of transparent ITO thin films range from 1.00×10^3 to 6.00×10^3 S cm^{-1} [20–23]. Hence, it seems that PEO–ITO nanocomposite thin films could be the good alternative of ITO films as transparent electrodes. Furthermore, the conductivity of PEO–ITO nanocomposites can be customized according to the requirement.

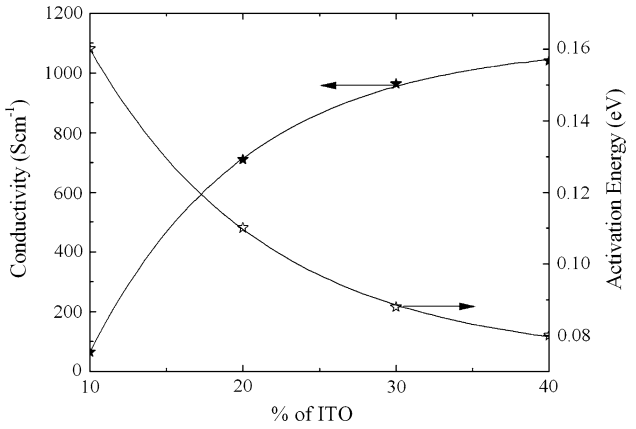

Fig. 5 Variations of conductivity and activation energy with ITO concentration

To find out the carrier transport mechanism of PI nanocomposite, the temperature dependence of conductivity was carried out within the range of 300–400 K for different samples. The activation energies for different PEO–PI nanocomposites were calculated from these conductivity versus temperature plots. Activation energy (Φ) decreases exponentially with the ITO concentration, as observed in Fig. 5. In fact, with the increase in ITO concentration, average separation between neighboring ITO particles in the PEO–PI nanocomposites reduces (Fig. 2), as a consequence Φ decreases, and conductivity enhances. Those facts suggest that the governing charge carrier transport mechanism in the PI nanocomposites is hopping conduction. We could find similar charge transport mechanism in "Coulomb glasses (metal–oxide composites)." Charge carriers in such systems are randomly localized in space. The long-range Coulomb interactions exist among the carriers. In the regime of strong Coulomb interaction the localization length of electron is much smaller than the distance between the localized states and the charge transfer is carried out by means of the tunnel hops of electrons from one center to another [24]. The activation energy for tunneling can be expressed by [25]

$$\Phi = \frac{144}{\varepsilon}\left(\frac{2}{r} - \frac{1}{(r/2+p)}\right)\text{eV}$$

where, r is the particle diameter, p is the separation between the particles both expressed in nanometers, and ε is the dielectric constant of matrix. In our case, instead of metal ITO particles are separated by the polymer tunneling. The current transport is considered by the tunneling of the carriers between the neighboring ITO dots in the PEO matrix. With the increase of ITO concentration, distance between the neighboring ITO particles decreases, activation energy lessens, and hence conductivity increases.

Conclusion

PEO–ITO nanocomposite templates were synthesized by the electrospinning. The properties of nanocomposites with various ITO concentrations have been studied. The structural studies show that the ITO particles of PEO–PI nanocomposites are distributed in a tangled network. The nanocomposites are optically transparent (85–90%) in the visible region (400–700 nm) of the solar spectrum. The variation of ITO concentration changes the electronic conductivity of the transparent nanocomposites. The highest conductivity achieved is 1.04×10^3 S cm^{-1} which shows the promise of PI nanocomposites to be used in place of ITO for the next generation photo devices.

References

1. Shalav A (2007) Prog Photovolt: Res Appl 15:275
2. Spanggaard H, Krebs FC (2004) Sol Energ Mater Sol C 83:125
3. Hartnagel HL, Dawar AL, Jain AK, Jagadish CJ (1995) Semiconducting transparent thin films. IOP, Bristol
4. Carter SA, Angelopoulos M, Karg S, Brock PJ, Scott JC (1997) Appl Phys Lett 70:2067
5. Sasaki M, Kieda N, Katayama K, Takeda K, Nakajima A (2004) J Mater Sci 39:3717. doi:10.1023/B:JMSC.0000030725.35826.77
6. Maruyma T, Fukui K (1991) J Appl Phys 70:3848
7. Căda M, Churpita O, Hubička Z, Hšíchová, Jastrabík L (2004) Surf Coat Technol 177–178:699
8. Schadler LS, Brinson LC, Sawyer WG (2007) J Miner Met Mater Soc 59:53
9. Clayton L, Sikder AK, Kumar A, Cinke M, Meyyappan M, Gerasimov T, Harmon JP (2005) Adv Funct Mater 15:101
10. Luo J, Glatkowski PJ, Wallis P (2005) US Pat Appl Publ (No. US 2005209392)
11. Moon JS, Park JH, Lee TY, Kim YW, Yoo JB, Park CY, Kim JM, Jin KW (2005) Diam Relat Mater 14:1882
12. Geblinger N, Thiruvengadathan R, Regev O (2007) Compos Sci Technol 67:895
13. Puetz J, Al-Dahoudi N, Aegerter MA (2004) Adv Eng Mater 6:733
14. Carotenuto G, Valente M, Sciumè G, Valente T, Pepe G, Ruotolo A, Nicolais L (2006) J Mater Sci 41:5587. doi:10.1007/S10853-006-0253-y
15. Materials Data, Inc. (1998) Computer software JADE, XRD pattern and processing & identification, Version 3.1
16. Watanabe K, Yamazaki T, Hashimoto I, Shiojiri M (2001) Phys Rev B 64:115432
17. Saq'an SA, Ayesh AS, Zihlif A (2004) Opt Mater 24:629
18. Zhang J, Au KH, Zhu ZQ, O'Shea S (2004) Opt Mater 26:47
19. Balasubramanian N, Subramanyam A (1989) J Phys D: Appl Phys 22:206
20. Kim JH, Ahn BD, Lee CH, Jeon KA, Kang HS, Kim GH, Lee SY (2007) Thin Solid Films 515:3580
21. Kim H, Horwitz JS, Kushto G, Piqué A, Kafafi ZH, Gilmore CM, Chrisey DB (2000) J Appl Phys 88:6021
22. Alia HM, Mohamed HA, Mohamed SH (2005) Eur Phys J Appl Phys 31:87
23. Lin T-C, Chang S-C, Chiu C-F (2006) Mater Sci Eng B 129:39
24. Fujii M, Mamezaki O, Hayashi S, Yamamoto K (1998) J Appl Phys 83:1507
25. Tick PA, Fehlner FP (1962) J Appl Phys 43:362